

# Highly Polarized Energetic Electrons via Intense Laser-Irradiated Tailored Targets

Xiaofei Shen,<sup>\*</sup> Zheng Gong, Karen Z. Hatsagortsyan,<sup>†</sup> and Christoph H. Keitel  
*Max-Planck-Institut für Kernphysik, Saupfercheckweg 1, 69117 Heidelberg, Germany*

(Dated: June 11, 2024)

A method for the generation of ultrarelativistic electron beams with high spin polarization is put forward, where a tightly-focused linearly-polarized ultraintense laser pulse interacts with a nonpolarized transverse-size-tailored solid target. The radiative spin polarization and angular separation is facilitated by the standing wave formed via the incident and reflected laser pulses at the overdense plasma surface. Strong electron heating caused by transverse instability enhances photon emission in the density spikes injected into the standing wave near the surface. Two groups of electrons with opposite transverse polarization emerge, anti-aligned to the magnetic field, which are angularly separated in the standing wave due to the phase-matched oscillation of the magnetic field and the vector potential. The polarized electrons propelled into the plasma slab, are focused at the exit by the self-generated quasistatic fields. Our particle-in-cell simulations demonstrate the feasibility of highly polarized electrons with a single 10 PW laser beam, e.g. with polarization of 60% and charge of 8 pC selected at energy of 200 MeV within 15 mrad angle and 10% energy spread.

Spin-polarized electron beams are an essential tool for physical research with applications spanning from particle physics [1–3] to material science [4–6]. Conventionally, spin-polarized relativistic electron beams are mainly produced via extraction from a photocathode [7] and further acceleration [8]. The alternative is radiative spin polarization (RSP) in storage rings [9–12]. However, both methods require unique and expensive large-scale accelerators, and the RSP in storage rings is rather slow. Recently, methods consisting of pre-polarizing a gas jet via photodissociation with circularly-polarized (CP) lasers and then accelerating them in a laser wakefield, were proposed [13–16], but multiple laser beams are required and the electrons are depolarized in the injection process. Such ideas are more refined in Refs. [17, 18] where polarized electrons are created during ionization injection of electrons with a CP laser into a particle-driven wakefield accelerator, but how to extend this to laser wakefields remains unclear.

With the rapid development of laser technology, PW and 10 PW laser facilities have been constructed worldwide such as [19–21], with a perspective for 100 PW [22–25]. Such intense laser pulses have important applications for nonlinear QED [23, 26, 27] including  $\gamma$ -ray [28–30] and pair production [31–35]. A question of growing interest is how to construct a laser-driven “mini-storage-ring” to efficiently polarize electrons via RSP in fs timescale by using ultrastrong laser fields. An additional highly polarized electron beam can significantly enhance research perspectives of a PW laser facility. Unfortunately, the basic concept of nonlinear Compton scattering in a strong monochromatic laser wave provides low polarization because of the oscillating character of the laser field: the polarization built up in a half-cycle is lost in the subsequent one [36–39]. To break the interaction symmetry and produce electron beams with net high spin polarization, several schemes have been proposed, such as colliding electron beams with elliptically-

polarized [40] or two-color [41, 42] pulses, and electrons trapped in the magnetic node of two colliding CP pulses [43–45]. However, experimental realization of the aforementioned schemes is still challenging, because it requires precise manipulation of laser polarization [22], or precise spatial and temporal control over multiple laser and electron beams [46, 47]. An especially limiting factor is the pointing stability of the beams.

The RSP in laser-plasma interaction (LPI) has been also analyzed recently [48–51]. In [48], polarized positron production in QED cascades is considered with a laser intensity  $I_L \simeq 3 \times 10^{24}$  W/cm<sup>2</sup>. There, the asymmetry for the spin-flip in the propagating laser wave stems from the wave damping due to pair production, which allows to induce net polarization of about 20%. The role of quasistatic magnetic fields in LPI for RSP has been investigated in Refs. [49–51] with an emphasis on applications for plasma diagnostics [49, 50]. The question of whether highly polarized dense relativistic electron beams could be obtained via intense LPI still remains open.

In this Letter, we investigate RSP of electrons via the interaction of an ultraintense tightly-focused linearly-polarized (LP) laser pulse with nonpolarized overdense plasma, see Fig. 1(a), aiming at highly polarized electrons with a single 10 PW-class laser beam. Particle-in-cell (PIC) simulations have been carried out with the EPOCH code [52], in which the radiative spin flips and spin precession have been implemented [49]. In the setup, the interaction symmetry is deliberately broken due to the reflection of the laser pulse at the overdense plasma boundary and the consequent formation of a standing wave. The strong transverse instability at the front surface [53, 54] gives rise to density spikes that penetrate into the stronger field region at the surface within a quarter-wavelength, where electron heating and photon emissions induce strong net RSP of electrons. The electrons are propelled into the plasma by light pressure without evident depolarization. They are split into two

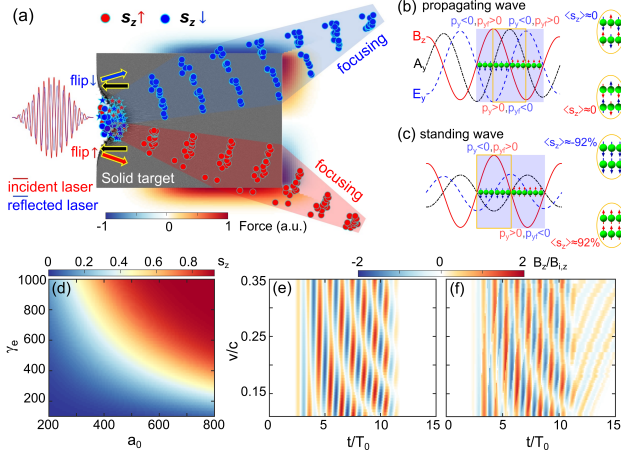


FIG. 1. (a) Interaction setup: an intense laser pulse impinges on a transverse-size-tailored solid target (gray). Counterpropagating electrons undergo spin-flip upon being pushed back into the target (arrows). Determined by instant local fields, the electrons have different divergences and are flipped to oppositely transverse polarization (pentagrams mark their initial positions). Upon exiting the target, a focusing force is self-generated confining the electrons. Illustration of the polarization and separation of electrons in a propagating (b) and standing (c) wave field, where  $p_y$  is the transverse momentum when the flip occurs and  $p_{yf}$  is the final momentum. (d) Theoretical estimation of  $s_z$  in a half-cycle using Eq. (2). Temporal evolution of  $B_z$  at  $x = 0$  for different hole-boring (HB) velocities: (e) theoretical prediction via Eq. (1), (f) via PIC simulations with parameters introduced in the text.

oppositely transversely-polarized parts because of the polarization and transverse momentum correlation in the standing wave field [Fig. 1(c)]. This contrasts to the case of a propagating wave [Fig. 1(b)], without transverse separation with respect to polarization. By transverse-size-tailoring (TST) of the target, the focusing of the polarized electrons at escaping the target is achieved by the self-generated quasistatic field. Despite of a broad momentum distribution of outgoing electrons, still the selection can yield a dense highly polarized relativistic electron beam, e.g., with the 10% energy and 15 mrad angular windows, an electron beam with 60% polarization, and 8 pC charge is obtained with a 10 PW laser.

We first consider a simplified model of our setup, where an ultraintense LP laser pulse, with vector potential  $A_{i,y} = a_0 \sin(x - t)$ , impinges on an overdense target. Here,  $a_0$  is the field amplitude, and dimensionless units are used:  $t \rightarrow \omega_L t$ ,  $x \rightarrow x\omega_L/c$ ,  $v \rightarrow v/c$ ,  $A_y \rightarrow eA_y/m_e c^2$ , where  $\omega_L$  is the laser frequency, while  $m_e$  and  $e$  are the electron mass and charge, respectively. The light pressure is known to induce HB effect, with the characteristic velocity  $v_{\text{HB}} = \sqrt{\Pi}/(1 + \sqrt{\Pi})$  [55], where  $\Pi = I_L/m_i n_i c^3$ ,  $m_i$  and  $n_i$  are the ion mass and density, respectively. The reflected laser pulse in the HB frame is [56, 57]:  $A'_{r,y} = a_0 \sin(x' + t')$  (the primed variables

belong to the moving frame), forming a standing wave:

$$\begin{aligned} A'_y &= 2a_0 \sin(x') \cos(t'), \\ B'_z &= 2a_0 \cos(x') \cos(t'), E'_y = 2a_0 \sin(x') \sin(t'). \end{aligned} \quad (1)$$

This would facilitate RSP: (i) The amplitude of  $B'_z$  is doubled, and it oscillates in phase with  $A'_y$  [Fig. 1(c)], different from the propagating wave [1(b)]; (ii)  $E'_y$  peaking at  $x' = -\pi/2$  would help confining electrons to a small region [58]; (iii) The pulse is “folded”, leading to highly asymmetric interaction.

For RSP,  $B_z$  is responsible, whose time evolution at  $x = 0$  for different  $v_{\text{HB}}$  is shown in Fig. 1(e). The “stripes” where the field is vanishing, originate from the time-varying  $v_{\text{HB}}$  and have been verified by our PIC simulations [Fig. 1(f)], where  $v_{\text{HB}}$  is manipulated via varying electron density  $n_e$ . The slower  $v_{\text{HB}}$  (higher  $n_e$  for the same  $I$ ), the fewer the “stripes”. Hence, employing high-density targets is beneficial for pursuing higher RSP.

Let us estimate RSP in our setup. Generally, at synchrotron motion, RSP is gradually built up according to  $s_z(t) = s_0 (1 - e^{-t/\tau_0})$  [12], with the characteristic polarization time  $\tau_0 = (8/5\sqrt{3})(m_e^2 c^2/e^2 \hbar)(R^3/\gamma_e^5)$ , and the RSP upper limit  $s_0 = 8/5\sqrt{3} \approx 0.9238$ . Here,  $\hbar$  is the reduced Planck constant,  $R$  the radius of the synchrotron motion, and  $\gamma_e$  the electron Lorentz-factor. Applying the synchrotron RSP in our case in the frame moving with  $v_{\text{HB}}$ , where the electron undergoes circular motion with  $R' = p'_\perp/(eB')$ , we arrive at the RSP time:

$$\tau_0 \approx \frac{8}{5\sqrt{3}} \frac{m_e^5 c^5}{e^5 \hbar} \frac{\gamma^3 \sin^3 \theta_e}{\gamma_e^2 B_z^3}, \quad (2)$$

where  $\gamma = 1/\sqrt{1 - v_{\text{HB}}^2}$  and  $\theta_e = \text{atan}(p_\perp/p_x)$  is the electron divergence angle. The RSP in a half-cycle, estimated by Eq. (2), which corresponds to the maximum achievable polarization in LPI, is shown in Fig. 1(d). The larger  $\gamma_e$  ( $a_0$ ), the higher  $s_z$  expected. With  $a_0 = 600$  and  $\gamma_e = 1000$ ,  $s_z$  reaches 91%, approaching the RSP limit of 92.38% [12]. Here we assume that electrons lose 50% energies to photons and  $\theta_e = 60^\circ$  obtained from simulations with immobile ions.

The estimation above is further proven by two-dimensional PIC simulations with realistic parameters. We use a laser pulse with peak intensity of  $5 \times 10^{23} \text{ W/cm}^2$  ( $a_0 = 600$  for a laser wavelength of  $\lambda_L = 1 \mu\text{m}$ ). The pulse is  $y$ -polarized with a transverse Gaussian profile and focal spot size  $d_L = 2 \mu\text{m}$ , duration of 15 fs with  $\sin^2$  temporal profile (feasible in upcoming 10 PW-class lasers [22, 23]). The initial phase is  $\pi$  to optimize the spin polarization. A uniform rectangular target is considered with thickness of  $9.4 \mu\text{m}$  and transverse size  $10 \mu\text{m}$  to focus electrons at about  $30^\circ$ , and  $n_e = 1200 n_c$  to maintain the target opaque without excessive computational efforts, where  $n_c = \pi m_e c^2/e^2 \lambda_L^2$  is the critical density. The restricted ion mobility is favorable, and considering the strong laser field, we have chosen the ion species

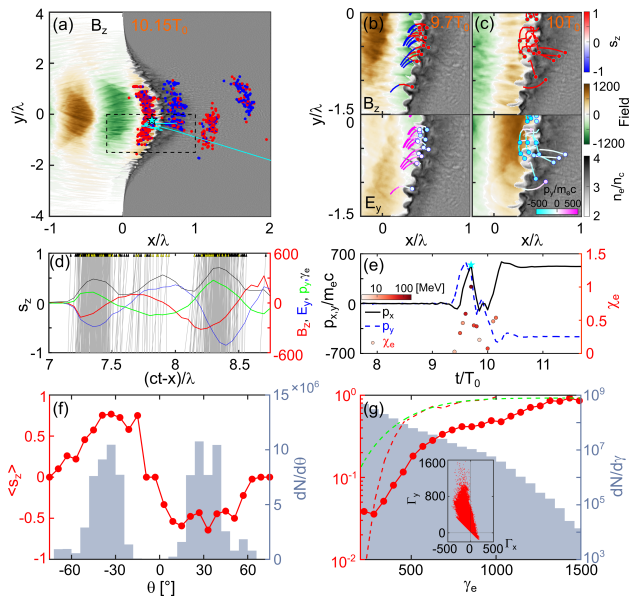


FIG. 2. Generation of highly spin-polarized electrons: (a) The laser pulse (contour) bores a hole on the target front (gray) when its peak arrives. The red (blue) dots present spin-up (down) electrons and the cyan line depicts a typical electron trajectory with details shown in (d) and (e). (b), (c) Snapshots to illustrate the correlation between electron emission direction and  $s_z$ , where the curves represent the electron trajectory within  $0.3T_0$  color-coded with their instant  $s_z$  (upper panel) and  $p_y$  (lower panel). (d) Evolution of  $s_z$  (gray), averaged  $p_y$  (green),  $B_z$  (red) and  $E_y$  (blue). The arrow color indicates the direction of final  $p_{yf}$  (black for  $p_{yf} < 0$ , yellow  $p_{yf} > 0$ ). Here only electrons with spin flipped up are shown. (e) Evolution of the electron momenta and  $\chi_e$  color-coded with the photon energy. The asterisks mark where (a) and when (e) its spin is flipped. (f) Angular distribution of  $\langle s_z \rangle$  (red dots) and electron number (blue) at the source for  $\gamma_e > 1200$ . (g) The corresponding  $\langle s_z \rangle$  and energy spectrum vs  $\gamma_e$  at around  $-32^\circ$ . The red dashed line shows the case with immobile ions (see Supplemental Materials (SM) [58]), while the green is the estimation using Eq. (2). The inset illustrates the energy-gain plane ( $\Gamma_x, \Gamma_y$ ) where  $\Gamma_{x,y} = -\int ev_{x,y} E_{x,y} dt$ .

to be  $\text{Au}_{197}^{69+}$  according to the Perelomov-Popov-Terent'ev ionization model [59, 60]. The simulation box ( $x, y$ ) is  $17.4\mu\text{m} \times 20\mu\text{m}$  with resolution of  $0.002\lambda_L \times 0.008\lambda_L$ . The macroparticles in each cell for electrons and ions are 1000 and 40, respectively. The pair production is neglected because their number is only 1% of high-energy electrons, and Bremsstrahlung plays a minor role for high-energy electrons traversing a thin foil [58]. Demonstrations of the robustness of our results (regarding effects of prepulse, oblique incidence, pointing stability, temporal profile, initial carrier envelope phase and 3D effects) as well as numerical convergence are presented in SM [58].

When a laser pulse irradiates an overdense plasma, transverse instabilities inevitably develop at the interface [53, 54], leading to the formation of density spikes, as shown in Fig. 2(a). These density spikes penetrate into

stronger field region, where electrons can be pulled out and accelerated to higher energies via  $\mathbf{j} \times \mathbf{B}$  heating, which is confirmed by the dominance of the transverse energy gain, see inset in Fig. 2(g) [58, 61]. The maximum electron energy exceeds 800 MeV [2(g)], much higher than the typical oscillating energy, even though radiation reaction (RR) takes away substantial energy. The electron quantum strong-field parameter  $\chi_e = (e\hbar/m_e^3c^4)|F_{\mu\nu}p^\nu|$  reaches about 1 [2(e)], with the field tensor  $F_{\mu\nu}$ , and the electron four-momentum  $p^\nu$ . The high-energy electrons in the strong field region have larger probabilities for RSP. Following the trajectory illustrated in Fig. 2(a) (cyan) and SM movie [58], most flips occur at the density spikes where the local field and  $\chi_e$  are stronger [2(e)].

The picture of the electron emission direction correlated with the spin polarization [Fig. 2(a-c)] has a simple explanation. It originates from the phase-matched oscillation in time of the magnetic field and the vector potential in a standing wave. The HB effect is minor for the polarization resolved angle separation (see the plane wave case in SM [58]). In RSP,  $s_z$  tends to flip to the opposite direction of  $B_z$  [upper panel in Fig. 2(b)], while  $p_y$  has the same sign as  $A_y$  (opposite to  $B_z$ ), see Eq. (1) and Fig. 2(d). Accordingly, the electron polarization and  $p_y$  at the photon emission are correlated, and the latter, along with the photon recoil, determines the final  $p_{yf}$  after the fast injection into the plasma [Fig. 2(c)] [58]. Consequently, in the plasma slab, the electrons with different polarization move in different transverse direction [Fig. 2(a)]. The angle between them is sufficiently large [Fig. 2(f)] to separate them in an experiment. We underline the difference from the propagating wave case [Fig. 1(b)], where for the given  $B_z$ , both signs of  $p_y$  are possible, hindering the separation over spin. Note that in our setup, the generation of hot electrons near the overdense target front and their injection into the plasma is an ultrafast process ( $< 1T_0$ ), during which each electron experiences only a single spin-flip and the spin depolarization is suppressed. This is because the electron energy is strongly reduced after the photon emission and the subsequent fields are much weaker [Fig. 2(e)]. This facilitates approaching the maximal theoretical RSP limit.

The RSP is created in a small region ( $< \lambda_L/4$ ) ahead of the HB front, and we evaluate the mean spin polarization  $\langle s_z \rangle$  created in this region (polarization at the source) in Fig. 2(g). Here,  $\theta_e = -32^\circ$ , where the electron polarization is highest and at  $t = 14T_0$ , when the RSP ceases. One can see that after the photon emission and injected into the plasma, the high polarization ( $s_z$ ) is still correlated with the high  $\gamma_e$ , similar to the theoretical prediction. The reason is that, when bounced back into the plasma, the electrons regain their initial energy [Fig. 2(e)]. With  $\gamma_e \sim 1000$  (1500),  $\langle s_z \rangle$  reaches about 50% (88%), approaching the upper limit of RSP. This is significantly higher than previous LPI schemes [48, 49]. Nevertheless, at the same  $\gamma_e$ , the polarization in the sim-

ulation is slightly lower than the theoretical limit [green in Fig. 2(g)]. This is because of the curved HB front. Electrons from the wings originate with moderate energies and stay in the laser field for longer time after the spin-flip, leading to slight depolarization.

For applications the polarization of the outgoing electron beam is important. Therefore, extracting the polarized electrons is crucial. For the standard transverse-size-unlimited target, outgoing electrons mainly experience longitudinal deceleration due to the sheath field established at the target rear [62, 63], which induces strong defocusing and greatly reduces the electron number at the angle of peak polarization, see Figs. 3(c-e).

The advantage of using the TST target is the focusing effect for the outgoing electrons due to the electrostatic fields induced at the target surface, as schematically illustrated in Fig. 1(a). This provides a new degree of freedom for manipulating the electron beam. Such targets are in use in current LPI experiments [64]. Figure 3(a) illustrates the force acting on the electrons traversing the target boundaries, where blue (red) indicates an inward (outward) scattering force. This is determined by comparing the instant  $\theta_e$  with the surface force direction  $\theta_f$ . It is clearly shown that at the corner, electrons are focused from both sides to around  $30^\circ$  [Fig. 3(b)].

The final polarization distributions of outgoing electrons collected at the simulation boundaries depending

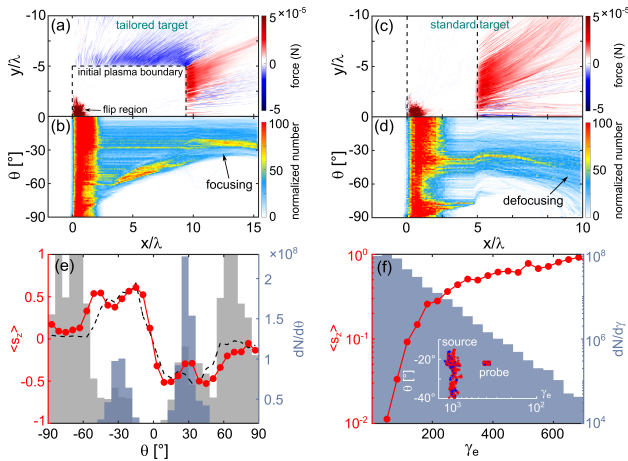


FIG. 3. Focus and collection of polarized electrons. (a) Trajectories of high-energy electrons with final  $\theta_e < 0^\circ$  color-coded with the instant force felt by them, where blue (red) represents an inward (outward) scattering force. (b)  $\theta_e$  vs  $x$ , where the colormap represents the relative electron number. (c,d) correspondingly show the results from the comparison case with a standard target. In (a,c), black dashed lines mark initial plasma boundaries. (e) Angular distributions of  $\langle s_z \rangle$  (red for TST, black for comparison case) and electron number (blue for TST, gray for comparison case) for electrons collected at the simulation boundaries with  $\gamma_e > 300$ . (f) The corresponding  $\langle s_z \rangle$  and energy spectrum vs  $\gamma_e$ . The inset displays the focusing of selected electrons with  $s_z$  color-coded.

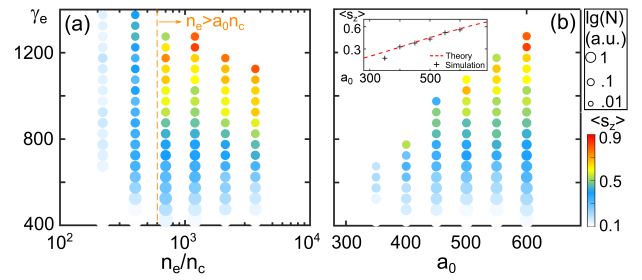


FIG. 4. Scaling. (a), (b) Dependence of  $\langle s_z \rangle$  on  $n_e$  (same  $a_0 = 600$ ) and  $a_0$  (same  $n_e = 1200n_c$ ). The marker size represents the charge. (c) Scaling of  $\langle s_z \rangle$  with respect to  $a_0$ , with  $\gamma_e > 1.5a_0$ : simulation (black crosses) and theory (red).

on  $\theta_e$  and  $\gamma_e$  are shown in Figs. 3(e) and 3(f). The electron number peaks at about  $\pm 30^\circ$  with narrower opening angles than at the source. By selecting  $\gamma_e > 200$ , 400 and 700,  $\langle s_z \rangle$  is about 40%, 60% and 90%, respectively. Thus, the TST target helps to focus electrons, but has no side effects on the polarization. The minor impact of the laser beam jitter on the focusing properties of TST target is discussed in SM [58]. In plasma-based electron acceleration, the number of low-energy electrons always largely exceeds that of high-energy ones regardless of acceleration mechanisms, but they are of little interest and cannot be polarized limited by Eq. (2). Thus, beam transport lines have been widely employed in laser wakefield acceleration to filter them out and improve the beam parameters [65–67]. By passing through the beam transport line developed in [65], it is feasible to select electrons at 200 MeV within 15 mrad and 10% energy spread [inset of Fig. 3(f)] without much loss. The beam charge still reaches approximately 8 pC and the polarization is about 60%. Note that without selection the total charge exceeds 110 pC at polarization 60%, and 2 pC at 90%. Compared to the standard case, the electron charge is about twice higher [Fig. 3(e)] and can be further enhanced by optimizing the target parameters.

The role of the plasma ( $n_e$ ) and laser ( $a_0$ ) parameters on RSP is analyzed in Figs. 4(a), (b). For  $a_0 = 600$  and relativistically-overdense plasma ( $n_e > a_0 n_c$ ), the physical process is similar and the maximum polarization can always reach above 80% at the high-energy part. However, for  $n_e < a_0 n_c$ , both the time and space scales of LPI are extended, and due to much weaker reflection, the interaction symmetry cannot be broken. Hence, the final polarization decreases, vanishing at  $n_e \ll a_0 n_c$ .

In Fig. 4(b),  $\langle s_z \rangle$  increases with  $a_0$  and  $\gamma_e$ , following the prediction of Eq. (2). We can provide analytical scaling for the average  $\langle s_z \rangle$  at  $\gamma_e > 1.5a_0$  and  $a_0 \in [350, 600]$  discussed here. From simulations we found that the factor of  $\gamma \sin \theta_e / B_z$  remains almost constant because an increase in  $a_0$  is accompanied by an increase of both  $\gamma$  ( $v_{HB}$ ) and  $\theta_e$  (caused by a deeper HB front). Consequently, the RSP time  $\tau_0 \propto 1/\gamma_e^2$  and  $P \approx P_0 [1 - e^{c_0(\gamma_e/100)^2}]$  with

$c_0 = -0.0121$  characterizing the polarization efficiency in a half-cycle. A good agreement of this analytical estimation with the simulation results is illustrated in the inset of Fig. 4(b). It shows that with a weaker laser field of  $a_0 = 400$  and higher energy selection  $\gamma_e > 2a_0$ , the polarization can still reach about 50%.

Concluding, we have shown the feasibility of producing highly polarized dense relativistic electron beams by using an upcoming 10 PW-class laser interacting with TST targets. Applying additionally a practical selection technique of the beam transport lines, high-energy low spread electron beams with polarization  $> 60\%$  and considerable charge are achievable, that are auspicious for extensive applications.

---

\* [shen@mpi-hd.mpg.de](mailto:shen@mpi-hd.mpg.de)

† [k.hatsagortsyan@mpi-hd.mpg.de](mailto:k.hatsagortsyan@mpi-hd.mpg.de)

- [1] G. Moortgat-Pick, T. Abe, G. Alexander, B. Ananthanarayan, A. A. Babich, V. Bharadwaj, D. Barber, A. Bartl, A. Brachmann, S. Chen, *et al.*, Polarized positrons and electrons at the linear collider, *Phys. Rep.* **460**, 131 (2008).
- [2] A. Accardi, J. Albacete, M. Anselmino, N. Armesto, E. Aschenauer, A. Bacchetta, D. Boer, W. Brooks, T. Burton, N.-B. Chang *et al.*, Electron-Ion Collider: The next QCD frontier: Understanding the glue that binds us all, *Eur. Phys. J. A* **52**, 268 (2016).
- [3] D. Abbott *et al.* (PEPPo Collaboration), Production of highly polarized positrons using polarized electrons at MeV energies, *Phys. Rev. Lett.* **116**, 214801 (2016).
- [4] R. Feder, *Polarized Electrons in Surface Physics* (World Scientific, Singapore, 1986), Vol. 1
- [5] S. A. Wolf, D. D. Awschalom, R. A. Buhrman, J. M. Daughton, S. von Molnár, M. L. Roukes, A. Y. Chtchelkanova, and D. M. Treger, Spintronics: a spin-based electronics vision for the future, *Science* **294**, 1488 (2001).
- [6] I. Zutic, J. Fabian, and S. Das Sarma, Spintronics: Fundamentals and applications, *Rev. Mod. Phys.* **76**, 323 (2004).
- [7] D. T. Pierce and F. Meier, Photoemission of spin-polarized electrons from GaAs, *Phys. Rev. B* **13**, 5484 (1976).
- [8] W. Hartmann, D. Conrath, W. Gasteyer, H. J. Gessinger, W. Heil, H. Kessler, L. Koch, E. Reichert, H. G. Andresen, T. Kettner, *et al.*, A source of polarized electrons based on photoemission of GaAsP, *Nucl. Instrum. Methods Phys. Res., Sect. A* **286**, 1 (1990).
- [9] A. A. Sokolov and I. M. Ternov, On polarization and spin effects in the theory of synchrotron radiation, *Sov. Phys. Dokl.* **8**, 1203 (1964).
- [10] A. A. Sokolov and I. M. Ternov, *Synchrotron Radiation* (Akademic, Germany, 1968).
- [11] V. N. Baier and V. M. Katkov, Radiational polarization of electrons in inhomogeneous magnetic field, *Phys. Lett.* **24A**, 327 (1967).
- [12] V. N. Baier, Radiative polarization of electron in storage rings, *Sov. Phys. Usp.* **14**, 695 (1972).
- [13] M. Wen, M. Tamburini, and C. H. Keitel, Polarized laser-wakefield-accelerated kiloampere electron beams, *Phys. Rev. Lett.* **122**, 214801 (2019).
- [14] Y. Wu, L. Ji, X. Geng, Q. Yu, N. Wang, B. Feng, Z. Guo, W. Wang, C. Qin, X. Yan, Polarized electron-beam acceleration driven by vortex laser pulses, *New J. Phys.* **21**, 073052 (2019).
- [15] M. Büscher, A. Hützen, L. Ji and A. Lehrach, Generation of polarized particle beams at relativistic laser intensities, *High Power Laser Sci. Eng.* **8**, e36 (2020).
- [16] H. C. Fan, X. Y. Liu, X. F. Li, J. F. Qu, Q. Yu, Q. Kong, S. M. Weng, M. Chen, M. Büscher, P. Gibbon, S. Kawata and Z. M. Sheng, Control of electron beam polarization in the bubble regime of laser-wakefield acceleration, *New J. Phys.* **24**, 083047 (2022).
- [17] Z. Nie, F. Li, F. Morales, S. Patchkovskii, O. Smirnova, W. An, N. Nambu, D. Matteo, K. A. Marsh, F. Tsung, *et al.*, In Situ Generation of High-Energy Spin-Polarized Electrons in a Beam-Driven Plasma Wakefield Accelerator, *Phys. Rev. Lett.* **126**, 054801 (2021).
- [18] Z. Nie, F. Li, F. Morales, S. Patchkovskii, O. Smirnova, W. An, C. Zhang, Y. Wu, N. Nambu, D. Matteo, *et al.*, Highly spin-polarized multi-GeV electron beams generated by single-species plasma photocathodes, *Phys. Rev. Research* **4**, 033015 (2022).
- [19] J. W. Yoon, Y. G. Kim, I. W. Choi, J. H. Sung, H. W. Lee, S. K. Lee, and C. H. Nam, Realization of laser intensity over  $10^{23} \text{ W/cm}^2$ , *Optica* **8**, 630 (2021).
- [20] F. Lureau, G. Matras, O. Chalus, C. Derycke, T. Morbieu, C. Radier, O. Casagrande, S. Laux, S. Ricaud, G. Rey, *et al.*, High-energy hybrid femtosecond laser system demonstrating  $2 \times 10$  PW capability, *High Power Las. Sci. Eng.* **8**, e43 (2020).
- [21] W. Li, Z. Gan, L. Yu, C. Wang, Y. Liu, Z. Guo, L. Xu, M. Xu, Y. Hang, Y. Xu, *et al.*, 339 J high-energy Ti:sapphire chirped-pulse amplifier for 10 PW laser facility, *Opt. Lett.* **43**, 5681 (2018)
- [22] C. N. Danson, C. Haefner, J. Bromage, T. Butcher, J.-C. F. Chanteloup, E. A. Chowdhury, A. Galvanauskas, L. A. Gizzi, J. Hein, D. I. Hillier, *et al.*, Petawatt and exawatt class lasers worldwide, *High Power Laser Sci. Eng.* **7**, e54 (2019).
- [23] A. Gonoskov, T. G. Blackburn, M. Marklund, and S. S. Bulanov, Charged particle motion and radiation in strong electromagnetic fields, *Rev. Mod. Phys.* **94**, 045001 (2022).
- [24] B. Shao, Y. Li, Y. Peng, P. Wang, J. Qian, Y. Leng, and R. Li, Broad-bandwidth high-temporal-contrast carrier-envelope-phase-stabilized laser seed for 100 PW lasers, *Opt. Lett.* **45**, 2215 (2020).
- [25] Exawatt Center for Extreme Light Studies (XCELS), <https://xcel.s.iapras.ru>.
- [26] A. Di Piazza, C. Müller, K. Z. Hatsagortsyan, and C. H. Keitel, Extremely high-intensity laser interactions with fundamental quantum systems, *Rev. Mod. Phys.* **84**, 1177 (2012).
- [27] A. Fedotov, A. Ilderton, F. Karbstein, B. King, D. Seipt, H. Taya, G. Torgrimsson, Advances in QED with intense background fields, *Phys. Rep.* **1010**, 1 (2023).
- [28] L. Ji, A. Pukhov, E. N. Nerush, I. Y. Kostyukov, B. F. Shen, K. U. Akli, Energy partition, gamma-ray emission, and radiation reaction in the near-quantum electrodynamic regime of laser-plasma interaction, *Phys. Plasmas* **21**, 023109 (2014).

- [29] A. Gonoskov, A. Bashinov, S. Bastrakov, E. Efimenko, A. Ilderton, A. Kim, M. Marklund, I. Meyerov, A. Muraviev, and A. Sergeev, Ultrabright GeV photon source via controlled electromagnetic cascades in laser-dipole waves, *Phys. Rev. X* **7**, 041003 (2017).
- [30] A. Sampath, X. Davoine, S. Corde, L. Gremillet, M. Gilljohann, M. Sangal, C. H. Keitel, R. Ariniello, J. Cary, H. Ekerfelt, *et al.*, Extremely dense gamma-ray pulses in electron beam-multifoil collisions, *Phys. Rev. Lett.* **126**, 064801 (2021).
- [31] H. X. Chang, B. Qiao, Z. Xu, X. R. Xu, C. T. Zhou, X. Q. Yan, S. Z. Wu, M. Borghesi, M. Zepf, and X. T. He, Generation of overdense and high-energy electron-positron-pair plasmas by irradiation of a thin foil with two ultraintense lasers, *Phys. Rev. E* **92**, 053107 (2015).
- [32] A. R. Bell and J. G. Kirk, Possibility of prolific pair production with high-power lasers, *Phys. Rev. Lett.* **101**, 200403 (2008).
- [33] C. P. Ridgers, C. S. Brady, R. Ducloux, J. G. Kirk, K. Bennett, T. D. Arber, A. P. Robinson, and A. R. Bell, Dense Electron-Positron Plasmas and Ultraintense rays from Laser-Irradiated Solids, *Phys. Rev. Lett.* **108**, 165006 (2012).
- [34] A. Di Piazza, Nonlinear Breit-Wheeler pair production in a tightly focused laser beam, *Phys. Rev. Lett.* **117**, 213201 (2016).
- [35] M. Vranic, T. Grismayer, R. A. Fonseca, and L. O. Silva, Electron-positron cascades in multiple-laser optical traps, *Plasma Phys. Controlled Fusion* **59**, 014040 (2017).
- [36] G. L. Kotkin, V. G. Serbo, and V. I. Telnov, Electron (positron) beam polarization by Compton scattering on circularly polarized laser photons, *Phys. Rev. ST Accel. Beams* **6**, 011001 (2003).
- [37] D. Yu. Ivanov, G. L. Kotkin, and V. G. Serbo, Complete description of polarization effects in emission of a photon by an electron in the field of a strong laser wave, *Eur. Phys. J. C* **36**, 127 (2004).
- [38] D. V. Karlovets, Radiative polarization of electrons in a strong laser wave, *Phys. Rev. A* **84**, 062116 (2011).
- [39] D. Seipt, D. Del Sorbo, C. P. Ridgers, and A. G. R. Thomas, Theory of radiative electron polarization in strong laser fields, *Phys. Rev. A* **98**, 023417 (2018).
- [40] Y.-F. Li, R. Shaisultanov, K. Z. Hatsagortsyan, F. Wan, C. H. Keitel, and J.-X. Li, Ultrarelativistic electron-beam polarization in single-shot interaction with an ultraintense laser pulse, *Phys. Rev. Lett.* **122**, 154801 (2019).
- [41] Y.-Y. Chen, P.-L. He, R. Shaisultanov, K. Z. Hatsagortsyan, and C. H. Keitel, Polarized positron beams via intense two-color laser pulses, *Phys. Rev. Lett.* **123**, 174801 (2019); H.-H. Song, W.-M. Wang, J.-X. Li, Y.-F. Li, and Y.-T. Li, Spin-polarization effects of an ultrarelativistic electron beam in an ultraintense two-color laser pulse, *Phys. Rev. A* **100**, 033407 (2019).
- [42] D. Seipt, D. Del Sorbo, C. P. Ridgers, and A. G. R. Thomas, Ultrafast polarization of an electron beam in an intense bichromatic laser field, *Phys. Rev. A* **100**, 061402(R) (2019).
- [43] D. Del Sorbo, D. Seipt, T. G. Blackburn, A. G. R. Thomas, C. D. Murphy, J. G. Kirk, and C. P. Ridgers, Spin polarization of electrons by ultraintense lasers, *Phys. Rev. A* **96**, 043407 (2017).
- [44] Q. Han, X. Geng, B. Shen, Z. Xu and L. Ji, Ultra-fast polarization of a thin electron layer in the rotational standing-wave field driven by double ultra-intense laser pulses, *New J. Phys.* **24**, 063013 (2022).
- [45] Q. Qian, D. Seipt, M. Vranic, T. E. Grismayer, T. G. Blackburn, C. P. Ridgers, A. G. R. Thomas, Parametric study of the polarization dependence of nonlinear Breit-Wheeler pair creation process using two laser pulses, *Phys. Plasmas* **30**, 103107 (2023).
- [46] K. Poder, M. Tamburini, G. Sarri, A. Di Piazza, S. Kuschel, C. D. Baird, K. Behm, S. Bohlen, J. M. Cole, D. J. Corvan, *et al.*, Experimental signatures of the quantum nature of radiation reaction in the field of an ultraintense laser, *Phys. Rev. X* **8**, 031004 (2018);
- [47] J. M. Cole, K. T. Behm, E. Gerstmayr, T. G. Blackburn, J. C. Wood, C. D. Baird, M. J. Duff, C. Harvey, A. Ilderton, *et al.*, Experimental evidence of radiation reaction in the collision of a high-intensity laser pulse with a laser-wakefield accelerated electron beam, *Phys. Rev. X* **8**, 011020 (2018).
- [48] H.-H. Song, W.-M. Wang, and Y.-T. Li, Dense polarized positrons from laser-irradiated foil targets in the QED regime, *Phys. Rev. Lett.* **129**, 035001 (2022).
- [49] Z. Gong, K. Z. Hatsagortsyan, and C. H. Keitel, Retrieving transient magnetic fields of ultrarelativistic laser plasma via ejected electron polarization, *Phys. Rev. Lett.* **127**, 165002 (2021).
- [50] Z. Gong, K. Z. Hatsagortsyan, and C. H. Keitel, Electron polarization in ultrarelativistic plasma current filamentation instabilities, *Phys. Rev. Lett.* **130**, 015101 (2023).
- [51] K. Xue, T. Sun, K.-J. Wei, Z.-P. Li, Q. Zhao, F. Wan, C. Lv, Y.-T. Zhao, Z.-F. Xu, *et al.*, Generation of High-Density High-Polarization Positrons via Single-Shot Strong Laser-Foil Interaction, *Phys. Rev. Lett.* **131**, 175101 (2023).
- [52] T. Arber, K. Bennett, C. Brady, A. Lawrence-Douglas, M. Ramsay, N. Sircombe, P. Gillies, R. Evans, H. Schmitz, A. Bell *et al.*, Contemporary particle-in-cell approach to laser-plasma modelling, *Plasma Phys. Controlled Fusion* **57**, 113001 (2015).
- [53] F. Pegoraro and S. V. Bulanov, Photon bubbles and ion acceleration in a plasma dominated by the radiation pressure of an electromagnetic pulse, *Phys. Rev. Lett.* **99**, 065002 (2007).
- [54] X. F. Shen, B. Qiao, H. Zhang, S. Kar, C. T. Zhou, H. X. Chang, M. Borghesi, and X. T. He, Achieving Stable Radiation Pressure Acceleration of Heavy Ions via Successive Electron Replenishment from Ionization of a High-Z Material Coating, *Phys. Rev. Lett.* **118**, 204802 (2017).
- [55] A. P. L. Robinson, P. Gibbon, M. Zepf, S. Kar, R. G. Evans, and C. Bellei, Relativistically correct hole-boring and ion acceleration by circularly polarized laser pulses, *Plasma Phys. Controlled Fusion* **51**, 024004 (2009).
- [56] A. Macchi, S. Veghini, and F. Pegoraro, "Light sail" acceleration reexamined, *Phys. Rev. Lett.* **103**, 085003 (2009).
- [57] I. Yu. Kostyukov and E. N. Nerush, Production and dynamics of positrons in ultrahigh intensity laser-foil interactions, *Phys. Plasmas* **23**, 093119 (2016).
- [58] The Supplemental Materials mainly include the details of the spin flip process and more discussions about the field structure of the standing wave, the electron heating/acceleration mechanism, the Bremsstrahlung effect, the robustness of our results including using a 5 PW laser pulse and considering different target materials,

- preplasma, oblique incidence, pointing instability, initial carrier envelop phase, and 3D, and the numerical convergence. The Supplemental Materials include Refs. [68]-[82].
- [59] A. M. Perelomov, V. S. Popov, and M. V. Terent'ev, Ionization of atoms in an alternating electric field, *Sov. Phys. JETP* **23**, 924 (1966); Ionization of atoms in an alternating electric field: II, *ibid.* **24**, 207 (1967).
- [60] M. V. Ammosov, N. B. Delone, and V. P. Krainov, Tunnel ionization of complex atoms and of atomic ions in an alternating electromagnetic field, *Sov. Phys. JETP* **64**, 1191 (1986).
- [61] P. Gibbon, *Short Pulse Laser Interactions with Matter* (Imperial College Press, London, 2005)
- [62] A. Macchi, M. Borghesi and M. Passoni, Ion acceleration by superintense laser-plasma interaction, *Rev. Mod. Phys.* **85**, 751 (2013).
- [63] X. F. Shen, A. Pukhov and B. Qiao, Monoenergetic high-energy ion source via femtosecond laser interacting with a microtape, *Phys. Rev. X* **11**, 041002 (2021).
- [64] S. Buffechoux, J. Psikal, M. Nakatsutsumi, L. Romagnani, A. Andreev, K. Zeil, M. Amin, P. Antici, T. Burris-Mog, A. Compant-La-Fontaine, *et al.*, Hot electrons transverse refluxing in ultraintense laser-solid interactions, *Phys. Rev. Lett.* **105**, 015005 (2010).
- [65] T. André, I. A. Andriyash, A. Loulergue, M. Labat, E. Roussel, A. Ghaith, M. Khojayan, C. Thauray, M. Valléau, F. Briquez, *et al.*, Control of laser plasma accelerated electrons for light sources, *Nat. Commun.* **9**, 1334 (2018).
- [66] J. van Tilborg, S. Steinke, C. G. R. Geddes, N. H. Matlis, B. H. Shaw, A. J. Gonsalves, J. V. Huijts, K. Nakamura, J. Daniels, C. B. Schroeder, *et al.*, Active Plasma Lensing for Relativistic Laser-Plasma-Accelerated Electron Beams, *Phys. Rev. Lett.* **115**, 184802 (2015).
- [67] A. R. Maier, N. M. Delbos, T. Eichner, L. Hübner, S. Jalas, L. Jeppe, S. W. Jolly, M. Kirchen, V. Leroux, P. Messner, M. Schnepf, *et al.*, Decoding sources of energy variability in a laser-plasma accelerator, *Phys. Rev. X* **10**, 031039 (2020).
- [68] K. Nakamura, H.-S. Mao, A. J. Gonsalves, D. E. Mittelberger, J. Daniels, A. Magana, C. Toth, and W. P. Leemans, Diagnostics, Control and Performance Parameters for the BELLA High Repetition Rate Petawatt Class Laser, *IEEE J. Quantum Electron.* **53**, 1200121 (2017)
- [69] T. Esirkepov, M. Borghesi, S. V. Bulanov, G. Mourou, and T. Tajima, Highly Efficient Relativistic-Ion Generation in the Laser-Piston Regime, *Phys. Rev. Lett.* **92**, 175003 (2004).
- [70] B. Dromey, S. Rykovanov, M. Yeung, R. Hörlein, D. Jung, D. C. Gautier, T. Dzelzainis, D. Kiefer, S. Palaniyppan, R. Shah, *et al.*, Coherent synchrotron emission from electron nanobunches formed in relativistic laser plasma interactions, *Nat. Phys.* **8**, 804 (2012).
- [71] H. Vincenti, Achieving extreme light intensities using optically curved relativistic plasma mirrors, *Phys. Rev. Lett.* **123**, 105001 (2019).
- [72] A. Lévy, T. Ceccotti, P. D'Óliveira, F. Réau, M. Perdrix, F. Quéré, P. Monot, M. Bougeard, *et al.*, Double plasma mirror for ultrahigh temporal contrast ultraintense laser pulses, *Opt. Lett.* **32**, 310 (2007).
- [73] Y. Huang, C. Zhang, Y. Xu, D. Li, Y. Leng, R. Li, Z. Xu, Ultrashort pulse temporal contrast enhancement based on noncollinear optical-parametric amplification, *Opt. Lett.* **36**, 781 (2011).
- [74] H. Kiriya, Y. Miyasaka, A. Kon, M. Nishiuchi, A. Sagsisaka, H. Sasao, A. S. Pirozhkov, Y. Fukuda, K. Ogura, K. Kondo, N. P. Dover, *et al.*, Enhancement of prepulse and picosecond pedestal contrast of the petawatt J-KAREN-P laser, *High Power Laser Sci. Eng.* **9**, e62 (2021).
- [75] P. Wang, Z. Gong, S. G. Lee, Y. Shou, Y. Geng, C. Jeon, I. J. Kim, H. W. Lee, J. W. Yoon, J. H. Sung, *et al.*, Super-heavy ions acceleration driven by ultrashort laser pulses at ultrahigh intensity, *Phys. Rev. X* **11**, 021049 (2021).
- [76] F. P. Condamine, N. Jourdain, J.-C. Hernandez, M. Taylor, H. Bohlin, A. Fajstavr, T. M. Jeong, D. Kumar, T. Lastovicka, O. Renner, S. Weber, High-repetition rate solid target delivery system for PW-class laser matter interaction at ELI Beamlines, *Rev. Sci. Instrum.* **92**, 063504 (2021).
- [77] F. Salvat, PENELOPE-2008: A Code System for Monte Carlo Simulation of Electron, Photon Transport (Nuclear Energy Agency, Barcelona, 2009).
- [78] G. R. Bluementhal, and R. J. Gould, Bremsstrahlung, synchrotron radiation, and Compton scattering of high-energy electrons traversing dilute gases, *Rev. Mod. Phys.* **42**, 237 (1970).
- [79] F. Wan, C. Lv, M. Jia, H. Sang and B. Xie, Photon emission by bremsstrahlung and nonlinear Compton scattering in the interaction of ultraintense laser with plasmas, *Eur. Phys. J. D* **71**, 236 (2017).
- [80] H. Olsen and L. C. Maximon, Photon and electron polarization in high-energy bremsstrahlung and pair production with screening, *Phys. Rev.* **114**, 887 (1959).
- [81] J. Beringer *et al.* (Particle Data Group), Review of particle physics, *Phys. Rev. D* **86**, 010001 (2012).
- [82] G. Alexander, J. Barley, Y. Batygin, S. Berridge, V. Bharadwaj, G. Bower, W. Bugg, F.-J. Decker, R. Dolan, Y. Efremenko, *et al.*, Undulator-based production of polarized positrons, *Nucl. Instrum. Methods Phys. Res., Sect. A* **610**, 451 (2009).